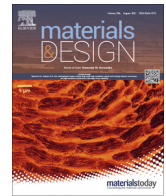Contents lists available at ScienceDirect

Materials & Design

journal homepage: www.elsevier.com/locate/matdes

Pressure and temperature sensitive e-skin for *in situ* robotic applications

Jarred W. Fastier-Wooller [a,c,*], Van Thanh Dau [a,d], Toan Dinh [b], Canh-Dung Tran [b], Dzung Viet Dao [a,c]

[a] School of Engineering and Built Environment, Griffith University, Southport, QLD 4222, Australia
[b] School of Mechanical and Electrical Engineering, University of Southern Queensland, Springfield Central, QLD 4300, Australia
[c] QLD Micro- and Nanotechnology Centre, Griffith University, Brisbane, QLD 4111, Australia
[d] Centre of Catalysis and Clean Energy, Griffith University, Australia

HIGHLIGHTS

- Development of a multimodal pressure and temperature sensitive e-skin.
- Successful integration on a curved surface via in situ electrospinning fabrication.
- Good performance and excellent stability over 1000 cycles.

GRAPHICAL ABSTRACT

CNT-PAN based sandwiched sensor: (i) conceptual design of our proposed sensor device and structure of sensing device, (iii) COMSOL simulation of concept sensor deformation under applied pressure, (ii), (iv) and (v) robot admiring new end effector sensors integrated with parallel gripper, with close-up of our *in situ* fabricated prototype sensor with Baxter robots end effector.
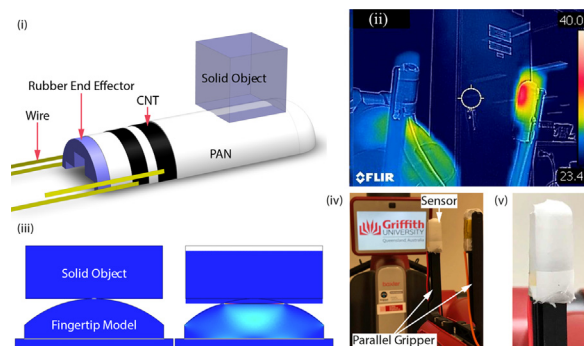
ARTICLE INFO

ABSTRACT

E-skin with physical sensing capability has attracted considerable interest towards practical applications in soft robotics, human–machine interfaces, and wearable health monitoring. However, the development of a multimodal sensing platform with multiple layers for e-skin sensing of temperature and pressure has faced challenges due to the typical use of bare or single sensing layers as well as the complication of integration of multifunctional sensing modules onto curved surfaces. Herein, we demonstrate a new platform technology with multiple sandwiched layers of highly oriented carbon nanotube (CNT) films and poly-acrylonitrile (PAN) for integration of pressure and temperature sensory functionalities into a single platform that is thin, ultra-lightweight, flexible, and wearable. The key technology of in-situ deposition of sensor platform on objects or in robot interface makes this a unique method for the development of e-skins for robotic applications, offering a new approach to wearable electronics and portable health care.

1. Introduction

There is an ongoing demand for smart multifunctional sensing capabilities in e-skins (electronic-skins) to aid further advancements in robotics designs and applications. Technology is

* Corresponding author.
  E-mail address: jarred.fastier-wooller@griffithuni.edu.au (J.W. Fastier-Wooller).

continually becoming more important in our daily lives, whether it be areas such as personal healthcare, workplace training, entertainment, or industry. To keep up with trends and advancements, design considerations and applications of robotics have been driven towards multimodal sensing capability, improved automation and artificial intelligence, ergonomic interaction between robotics and humans, and even the utilisation and manipulation of green materials and lifeforms [1–7].

E-skins and their materials are of continued considerable interest in the science and engineering community and tend to focus on stress/strain and pressure sensing, temperature, humidity, and other physical signals. In robotics applications, e-skin devices have been used to demonstrate a more advanced, functional, and versatile platform to perform these key measurements, mainly pressure and temperature measurements. Two common areas of e-skin development that are of great ongoing importance and interest involve personal health monitoring and robotics [8,9]. In human–machine interactions, a positive experience is more likely to impact a customer or patients' overall comfort and satisfaction, this is especially apparent in retail, recreational, and medical environments. As such, of notable importance in these applications is tactile sensing for robotic interaction with external objects, including pick and place and human–machine interaction.

Recent works in e-skin technologies have been focusing on improvements in performance (e.g. highly sensitive, thin, attachable), which is done via complex fabrication methods or rational design. Some of such works have shown a wide range of high performing devices using complex fabrication methods to create micro and nano structured pillars [10–12] and bumps [13] to improve sensitivity. J.C. Yang et al. present an even more complex sensing structure that takes advantage of increased porosity and pyramid-type structures by combining the two together, showing a sensitivity increase of over 2 times compared to that using solid pyramid structures [14]. D. Kwon et al. have presented an increase in sensitivity of their device, up to 38 times larger using a porous dielectric in place of a solid dielectric. The presented sensor is comparatively quite thick, at approx. 10 mm when uncompressed, and has the capability of detecting pressures in a wide range of 0.1 Pa to 130 kPa [15]. J. Jia et al. demonstrated a skin-inspired pressure sensor, using wrinkled rGO films sandwiched between electrodes. The porous structure of this device is reported to enable an ultra-high sensitivity of 178 kPa^{-1} [16]. At the cost of complexity of fabrication and integration, these works are highly indicative of the potential of thin and porous sensor design for a wide measurement range and excellent sensitivity.

However, little progress has been shown *in situ* fabrication for full integration of sensors into existing devices. E-skin research can be classified as make-and-transfer which has difficulties for sensor integration due to adhesion on curved and non-uniform surfaces. Sensors that use a make-and-transfer method are fabricated in sheets or packages and transferred to the surface of another device. Works have focused on altering designs and material selection to better adhere and integrate sensors [17–19]. Performing *in situ* fabrication is desired for e-skin because it requires very thin sensing layer that is conformally integrated over different geometry surfaces, this poses improvements to comfort, adhesion, and durability.

In this work, a thin and porous multimodal pressure and temperature sensitive e-skin is developed using a multi-layer structure of carbon nanotube (CNT) films and polyacrylonitrile (PAN). We employ electrospinning for *in situ* fabrication of the e-skin with its capability of integration on existing devices. Our sensitive e-skin device can be either manufactured and then transferred to surfaces or fabricated directly on the rubber end effector of a robot

gripper, showing a simple *in situ* fabrication process with a high aptitude for a broad range of robotic applications. The present *in situ* fabricated sensor can achieve a pressure sensitivity of up to 0.63% kPa^{-1} and a temperature coefficient of resistance (TCR) of –800 ppm K^{-1}. Due to the flexibility, strength, and structure of the materials used, very little damage results in overloading these devices. Our device demonstrates this with an excellent signal repeatability and stability over 1000 cycles. The porosity shows benefits to ease of deformation and ability to return to original state without compromising the thin structure of our device. By relevant preparation and fitting of temporary electrically conductive plates, experimental observations showed the ability to fabricate sensors directly onto an existing device using the present technique. Thus, our device is shown to be versatile in applications of *in situ* integration into existing devices and systems.

2. Design

To demonstrate the *in situ* fabrication method, the Baxter robot was nominated. Baxter (Rethink Robotics) is a robot with two arms, each capable of 7 degrees of freedom, designed for industry use with the safety of working alongside humans in mind. With a maximum reported force of the Baxter robots electric parallel gripper being 11 N [20], an estimated maximum gripper pressure of up to approx. 80 kPa is expected from being in contact with the entirety of the gripper surface to holding an object such as a pen at full force. The Baxter robots curved rubber end effectors are used in this work as the pre-existing platform. The rubber end effector would not be ideal for make-and-transfer style sensors due to issues adhering the surfaces of the sensor and fingertip without impacting on the sensing performance and physical properties. Attaching a very thin sensor that conformably covers the end effector is desirable to minimally impede the devices gripping ability, which is not available so far. Two ultra-lightweight and highly flexible materials that are able to contour to the surface of the end effector like a layer of skin were chosen as the base of our multi-layered capacitive and resistive device. The chosen materials are CNT and PAN, where CNT is used as a conductor and PAN as a dielectric.

The features by the sandwiched structure and the selected materials allow our device to have two main functions, to sense pressure and temperature, without additional circuitry or complex fabrication procedures. The structure of our device was designed to measure pressure (capacitance) between the two CNT layers which are separated by a soft porous layer of PAN, whereas the temperature (resistance) can be measured by the effect of temperature on a layer of CNT and by the change within capacitance caused by the variance of permittivity as well as any physical deformation of PAN due to thermal expansion. The outermost CNT layer protected by an ultra-thin and porous PAN layer allows heat to transfer through but protects the dedicated CNT temperature sensor (Fig. 1(i)).

Any combinations of three among four electrodes A, B, C, and D, shown in Fig. 1(ii), are required for both temperature and pressure sensing functionality. The introduction of a fourth electrode allows the measurement of temperature at both layers of the sensor device. The design concept when a curved and soft rubber end effector (i.e. robot finger) grasps a solid object was simulated using COMSOL (COMSOL Multiphysics v.5.2) in which the deformation of the robot finger was implemented with hyper-elastic model and the Young's modulus of the end effector is E = 4.1 MPa (silicone rubber material).
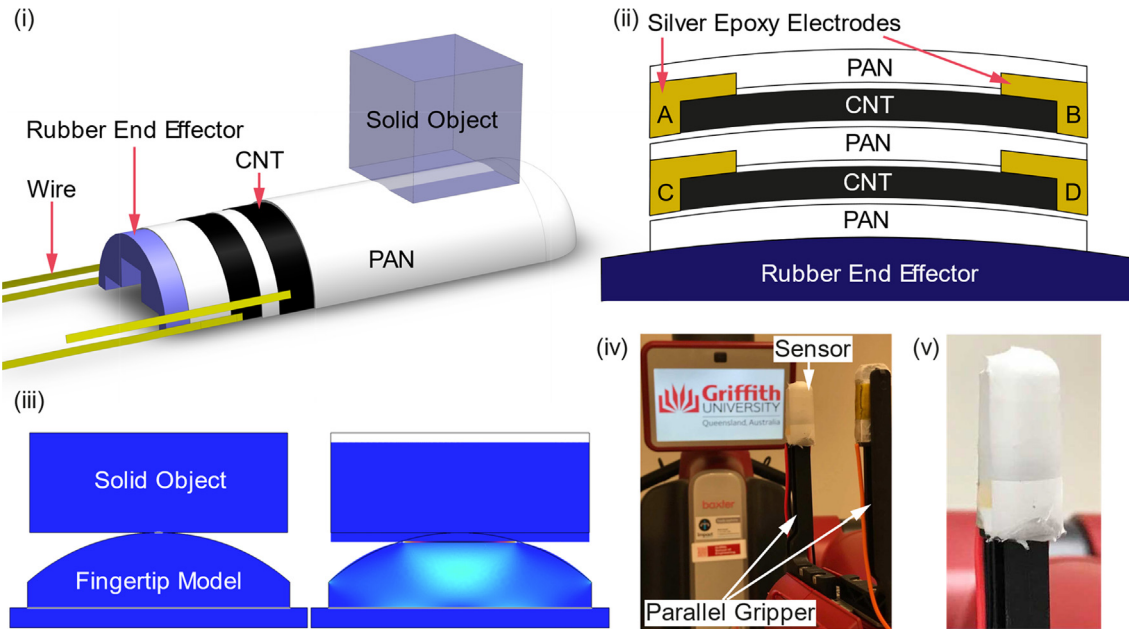
Fig. 1. CNT-PAN based sandwiched sensor: (i) conceptual design of our proposed sensor device, (ii) structure of sensing device, electrodes A-B for sensing temperature and electrodes B-C for sensing pressure, electrode D optional, (iii) COMSOL simulation of concept sensor deformation under applied pressure, (iv) Baxter robot admiring new end effector sensors integrated with parallel gripper, (v) close-up of our *in situ* fabricated prototype sensor with Baxter robots end effector.

3. Sensing principle

3.1. Capacitive pressure sensors

Due to the many micro-strands of layered PAN, there is a highly porous and flexible dielectric layer between two CNT layers in our device. The CNT layers provide a surface area separated by a porous PAN dielectric to form a capacitor. Capacitive sensors rely on a dielectric materials ability to hold/store charge or a change in permittivity to perform measurements of physical phenomena. This can be performed by varying the distance between the two conductive CNT layers on either side of the porous PAN dielectric. The formula for this is well known as,

$$C_o = \frac{q}{V} = \varepsilon \frac{A_o}{d_o} \qquad (1)$$

where d_o is the distance between CNT layers, q the charge between CNT layers, V the voltage between CNT layers, ε the permittivity of the material between the CNT layers, and A_o the area of overlap between two CNT layers. Generally, the permittivity remains constant at the same temperature and the main contributing factor is the change in distance between CNT layers. However, it should be noted that due to the PAN layer being highly porous, pressure variation causes the air between strands of PAN is shifted and expulsed which will contribute to a change in permittivity. It is expected that under direct pressure, the PAN layer is compressed and the physical change in the distance d will be the leading cause of the capacitance to increase. The application of pressure also deforms the soft base of the finger and thereby increases facing area, so the capacitance C between the two CNT layers increases. Thermal expansion of the physical structure can potentially contribute a relatively large impact on the output of the capacitive component. Thermal expansion of PAN is shown to have a single linear region between 20 and 90 °C [21], containing the area of interest of this research, this will have an effect on the distance between electrodes and the material to air ratio of the porous layers. We estimate an effect on distance d of approx. 0.007% K^{-1}, as the material will attempt to expand outwards, we assume d will increase, reducing the overall capacitance with temperature [21].

It can also be seen that as temperature changes, the permittivity can also change, as reported for thin film, ionic liquid (IL), tropospheric air, and PAN materials [22–25]. The effects of temperature on the permittivity can cause changes in capacitive output even in materials with a low temperature coefficient. We estimate the effect of temperature on the permittivity $\beta = (\Delta\varepsilon/\varepsilon)/\Delta T$ of air gaps [24] and PAN [25] to be approx. –0.371% K^{-1} and 0.597% K^{-1} respectively, showing a higher likelihood of capacitance increasing with temperature. From this we can also theorise that there will be an unavoidable effect due to humidity on capacitive measurements. In our application, we recommend that it is a simple task to fabricate and use another sensing device near the robot end effector to eliminate these effects and compensate for changes in humidity.

The effect of temperature can affect the output of the sensor as seen in Eq. (1). Thus, the main temperature dependence can be shown by

$$C = C_0(1 + \gamma \cdot \Delta T) \qquad (2)$$

where C_0 is the initial capacitance, γ is the temperature coefficient of capacitance, and ΔT is the change in temperature.

Thus, when touching an object that has a different temperature to the sensor, the capacitance pickup can therefore be represented as

$$\frac{\Delta C_{P,T}}{C_0} = \frac{Ad_0 - dA_o}{A_0 d} + \gamma \cdot \Delta T \qquad (3)$$

3.2. Resistive temperature sensors

Physical deformation in the material caused by stress/strain, force/pressure, and even temperature, cause the size/dimensions to change, resulting in a change in the electrical resistance R. These phenomena can be represented by

$$R = l/A\sigma \qquad (4)$$

where σ is the conductivity, l is the length, and A is the cross-sectional area of the material.

However, an ultrathin and well aligned CNT layer would be insensitive to a perpendicular applied pressure, but it is still sensitive to a change in temperature. Due to the highly oriented and porous structure of CNT used in our sensor, the effects of pressure and physical deformation perpendicular to the sensor surface has a negligible effect on resistance and will be observed further in Fig. 6. CNT has a reported TCR of −750 ppm K^{-1} [26], and it is capable of providing a stable temperature reading. The internal CNT temperature reading can be used in conjunction with the pressure reading to provide thermal compensation without the need for additional sensors or circuitry.

We hypothesize that the carriers are trapped in the CNT defects and disorders [27]. When the temperature increases, these trapped carriers are excited by the thermal energy, leading to an increase in the conductivity of the CNT and a negative TCR of the sensor. The electrical resistance of our sensor can thus be described as

$$R = R_c + \frac{1}{|t^2|}\left(\frac{h}{8e^2}\right)\left[1 + exp\left(\frac{E_{gap}}{kT}\right)\right] \tag{5}$$

where R_c is the contact resistance between CNT film and electrode, which is neglected, h and e are Planck's constant and primary charge, and $|t^2|$ is the probability of transferring an electron over the band gap of CNT with an energy of E_{gap}. This equation further suggests a decrease of the electrical resistance with increasing temperature and is indicative of a non-linear component. In a narrow range of temperature changes (e.g. 25 °C to 55 °C), the main temperature dependence can be linear as shown by

$$R = R_0(1 + \alpha \cdot \Delta T) \tag{6}$$

where R_0 is the initial resistance, α is the temperature coefficient of resistance (TCR), and ΔT is the change in temperature. Similarly, by substituting R for ρ the effects of temperature on the resistivity of the material can be seen.

4. Materials and fabrication

CNT has some interesting and impressive physical properties including a high elastic modulus of over 1 TPa, tensile strength of up to 100 GPa, and thermal conductivity of 3500 W m^{-1} K^{-1}. Excellent electrical properties such as an electrical conductivity of 2x10^7 S m^{-1}, ampacity up to 1013 A m^{-1}, and have a low impedance at high frequencies [28]. Fig. 3 shows a TCR value of approx. −800 p pm K^{-1}, similar to those of CNT reported in other works [29]. CNT was elected as the conductor for our sensor due to its flexibility, highly versatile properties, and conductivity.

CNT films were stretched, layered on, and wrapped around our sensor as the conductive medium. This was performed to achieve a soft, porous, and versatile surface electrode area. Raman measurements were performed to confirm the characteristics of the stretched layer CNT film. Fig. 2 (v) shows the two dominant peaks at the wavenumbers of 1345 and 1580 cm^{-1}, respectively representing the D and G bands of carbon materials. CNT is very thin and very light and as such is a good material for use as a flexible electrode. However, CNT membranes are not suitable for direct physical contact such as touching or pressing. A robust, low-cost, insulating, porous, lightweight, and thin material is ideal to protect and serve as dielectric layer.

PAN is as an insulating and non-corrosive material well suited for a capacitor's dielectric and protective layers. PAN has been chosen due to its similarly favourable flexible and versatile properties and the highly porous structure gained through the electrospinning fabrication process. To protect and separate the conductive layers to perform capacitive pressure measurements, layers of a synthesized PAN fibre network are used to cover the CNT membranes.

Our presented sensor is fabricated in situ on a robot end effector. However, by modifying the PAN delivery process we believe it is possible to perform fabrication directly on human skin. As stated by Senthilkumar et al., PAN is biocompatible and can be attached on the human body without any adverse impacts on human skin and the immune systems [30].

Fabrication of our sensing device is performed in situ on an existing device (Baxter Robot end effector) by electrospinning PAN onto the surface of the end effector to serve as the foundation (Fig. 2(i)). A layer of CNT is stretched from a CNT forest over the PAN layer leaving a small gap on the non-sensing side for electrode application (Fig. 2(ii)), further demonstration of placing CNT forest film and the control of its properties can be seen in our previous works [31,32]. A layer of PAN is spun over the CNT as the dielectric layer. To avoid any shorting between CNT layers when connecting the electrodes, an insulator (Kapton polyimide tape) is applied over the areas where the electrodes will be attached before the second CNT layer is applied. A final layer of PAN is introduced to encase and protect the sensor device. Parts of the PAN are carefully removed by a scalpel before adhering one electrode using silver epoxy to each layer of CNT for pressure sensors or two on each layer for pressure and temperature sensing. The silver epoxy permeates through the porous fibres of the PAN and CNT to form robust electrical contacts.

The demonstrated sensor is fabricated as an example for robot applications. The Baxter Robots curved rubber end effector was utilized to demonstrate our fabrication method and results. However, it is also possible to perform fabrication on a substitute substrate and transfer the sensing device to another surface or device. This is performed by electrospinning PAN onto the surface of a removable fabrication drum and repeating the same fabrication steps as per the in situ method. The device is peeled from the fabrication drum and then applied to another surface or device. This method can also be extended to fabrication of wearable electronics on the surface of the skin wherein the PAN is physically spun around the substrate.

5. Characterization and results

Testing of the fabricated device samples (as shown in Fig. 1(iv-v)) have been categorized into the following figures (Figs. 3–7). Initial demonstration and testing of the capacitive response to applied pressure on a curved surface using known weights was performed on a sample to gauge the success of the fabrication process and feasibility for pressure sensing.

Initial testing of the first sample fabricated on the surface of the Baxter Robots curved rubber end effector showed discrete and well distributed pressure measurements. For calibration purposes, measurements were performed using known weights. Weight was applied to the sensing area using a contoured acrylic cut-out designed to fit the Baxter robot's end effector with a constant and known surface area. Due to the nature of testing method, only measurements of up to 11.6 kPa are available. A sensitivity to pressure of up to 0.63% kPa^{-1} and a TCR of approx. −800 ppm K^{-1} are observed by the sensing device (Fig. 3). The response time of pressure is shown to be <1000 ms (Figure S1), which can be seen to be limited by the sampling rate of the testing equipment. Response time of temperature is evaluated by initial change in temperature on contact and can be seen to be as fast as <250 ms, limited by sample rate, with an overall response time of <750 ms (Figure S2).

The resistive elements in our sensing device were tested as heating elements. This was performed by supplying a constant current of 30 mA to the top layer of CNT, schematic can be seen in
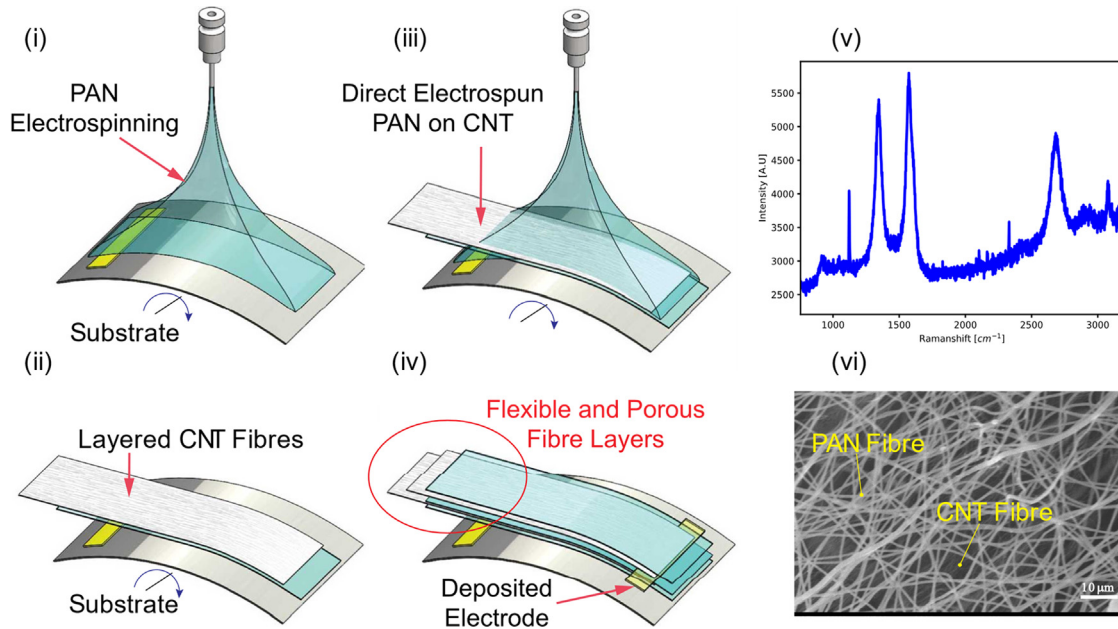
Fig. 2. Formation of CNT-PAN sandwiched sensor: (i–iv) illustration of fabrication process, (i) electrospinning process to apply PAN to substrate, (ii) CNT is laid over the PAN layer of device, (iii-iv) repeat steps in i-ii. (v) Raman spectroscopy of CNT used in the fabrication of our device. (vi) SEM image of flexible and porous PAN and layered CNT fibres.
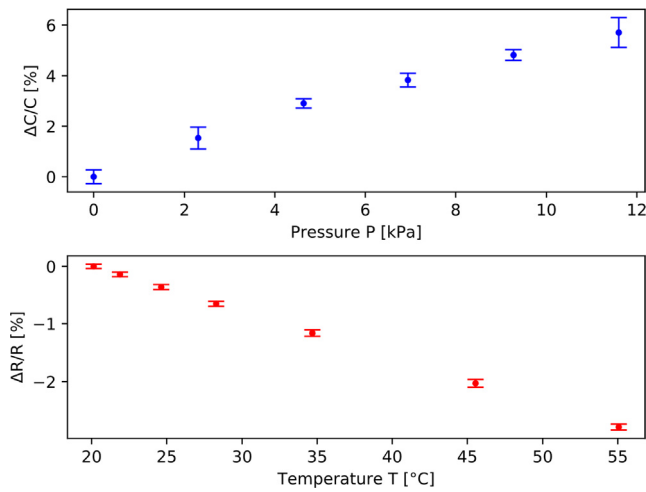
Fig. 3. Initial calibration and test of *in situ* fabricated sample on the Baxter robots selected rubber end effector using known weights. ΔR/R and ΔC/C are the relative changes in resistance and capacitance.

Fig. 4(i). Our experimental results showed that the fingertip sensor can not only be used as a temperature sensor, but each layer can also be used as a heating element. This would allow the fingertip to be tuned to a human-like temperature as necessary for human-robot interactions, providing a more human friendly interface subjectively compared to that of interactions with a cold device [33,34]. Fig. 4(ii, iii) shows thermal images (Flir C2 infrared camera) of our device matching the temperature of human skin, as can be seen in close proximity to a human fingertip. In Fig. 4(i), the addition of a current source to the measurement circuit produces heating capability without having a noticeable impact on the temperature sensing capability of the top layer. However, there is also potential for the bottom layer of CNT to be used as heating element while the top CNT layer is used to sense differential temperatures between the fingertip and contact temperatures, this would require an additional fourth electrode. The temperature sensing layer can be used independently or to regulate the temperature control of the heating layer.

Cycle testing was performed by repeatedly gripping and releasing a static object. The performance of the sensor shows high stability over a long period of time and cycles, demonstrated by the device in Fig. 5. The effects of thermal stress and additional defects introduced from cycle testing are believed to have a minor effect

Fig. 4. Experiment: Robot finger shown used in heating mode. (i) test circuit used, (ii) non-heated (left) and heated (right) robot fingers on Baxter's end effector, (iii) robot finger temperatures capable of matching that of human skin.
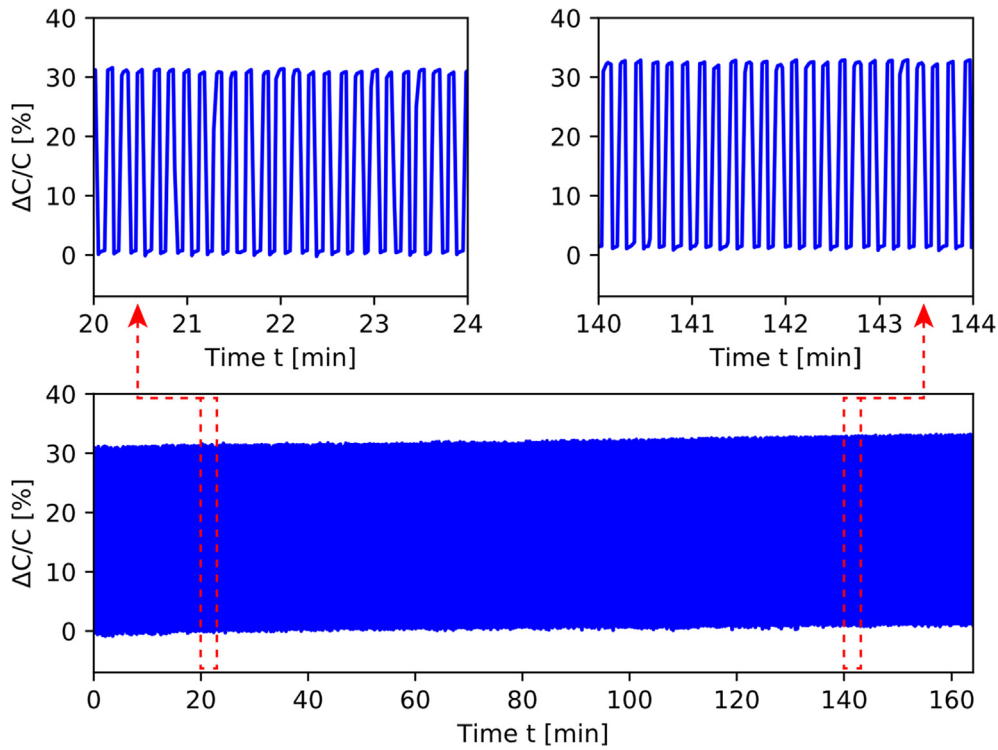
Fig. 5. Pressure cycles performed over 1000 cycles using the Baxter robot parallel gripper at maximum possible output. Top two graphs show additional signal detail near the start and end of cycle testing. Estimated gripping force, F ≈ 11 N. Estimated gripping pressure, P ≈ 70 kPa.

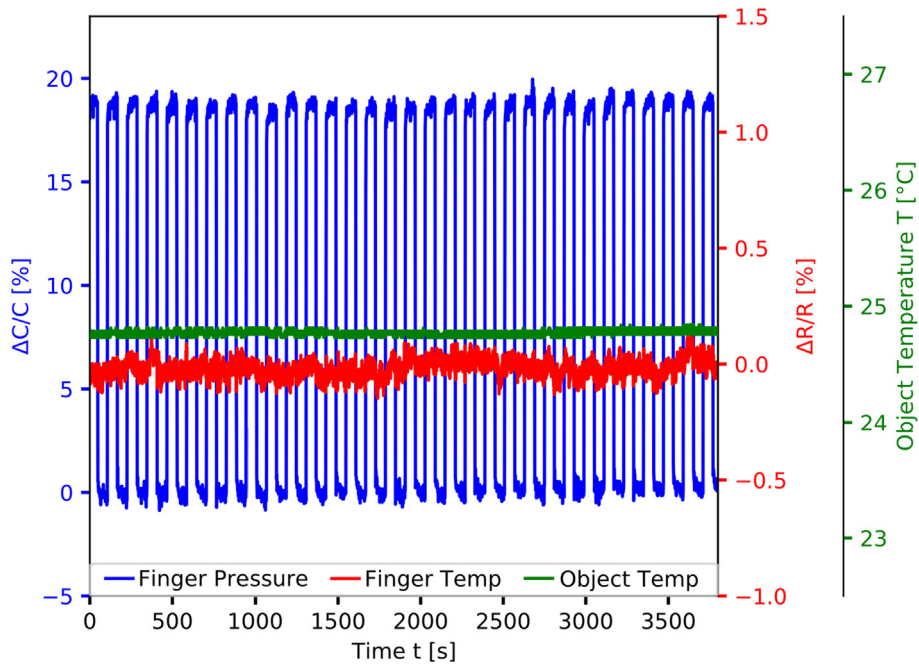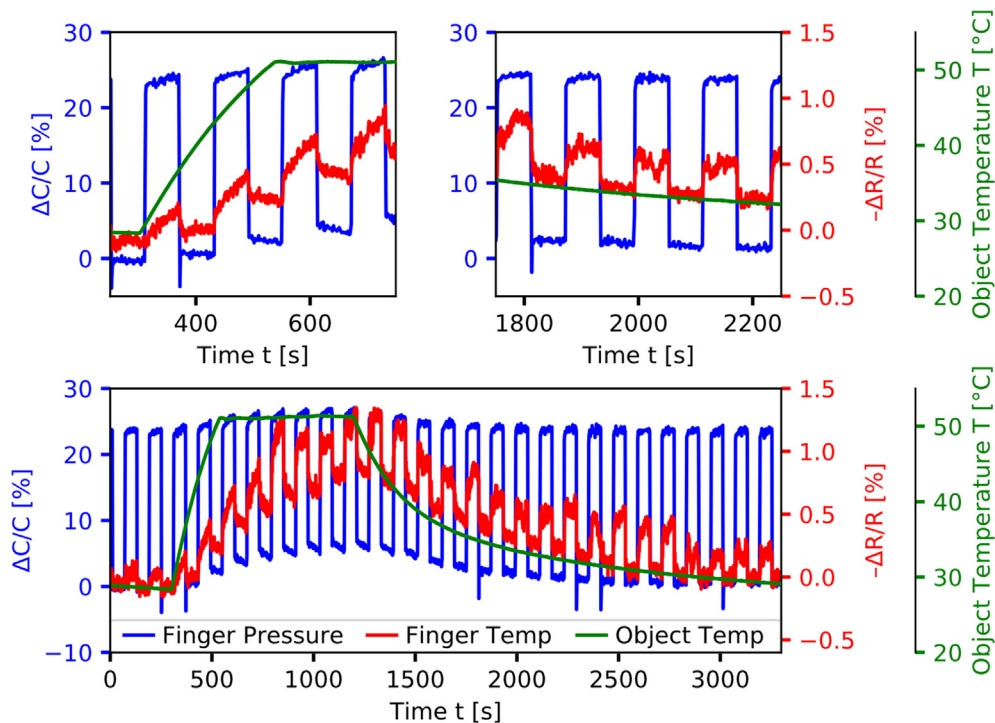**Fig. 6.** Cycle testing, gripping a solid aluminium cube in a temperature-controlled environment. Varying temperature of gripped object, ΔT ≈ 0.0 °C. Ambient temperature, T = 24.8 °C. Estimated gripping force, F ≈ 11 N. Estimated gripping pressure, P ≈ 48 kPa. Object is kept at room (ambient) temperature.

on the sensor's performance, shown by a uniform drift of approx. 0.4% with less than 0.7% change in magnitude over 100 cycles.

Repetitive grasping at a constant temperature was performed to demonstrate the effect of pressure on the resistance. The grasped object maintains a differential of 0 °C between the object and room temperature. Grasping is easily recognizable by the sharp increase of the measured capacitance. The grasping capacitance signal is stable, and sensitivity does not change. Temperature resistance measurements in the sensor are stable, with minor noise of ±0.1%.

Repetitive grasping was performed while the gripped objects temperature was varied from slightly above ambient room temperature to 50 °C. A sharp increase and decrease of resistance aligning with the sharp increase and decrease of pressure can be found in Fig. 7, this is caused by the sudden increase and decrease of tem-

Fig. 7. Cycle testing, gripping a solid aluminium cube in a temperature-controlled environment. Varying temperature of gripped object, $\Delta T \approx 20.0$ °C. Ambient temperature, T = 24.8 °C. Estimated gripping force, F $\approx$ 11 N. Estimated gripping pressure, P $\approx$ 60 kPa.

perature when the gripper comes in contact and releases the heated object. Figure S3 shows the effect on resistance and capacitance with a constant gripping pressure under varied temperature. The opposite effect can be seen in Figure S4, where the sensor device is used as the heating element. A difference in the ambient temperature around the object and the direct surface temperature of the object causes these peaks. Using the average expected TCR of our sensor, derived from Fig. 3, the peak measured temperature seen in Fig. 7 is estimated to reach 46 °C. From the estimated effects of temperature on the output of the materials in the sensor, we can approximate that the overall change in capacitance should be approx. 0.39% K^{-1} or 6.8%, an actual capacitance drift of $\approx$0.35% can be seen in Fig. 7. Sensitivity to pressure can also be seen to be affected by temperature $\approx$0.6% K^{-1}. Using the information from the temperature sensor it is very possible to compensate for this drift. Figure S5 shows an example of simple linear compensation using the data from Fig. 7. A similar process can be done to compensate for the effect of humidity by using an unloaded section of the capacitive component as a humidity sensor (additional electrodes required).

6. Conclusions

We have successfully demonstrated the design, fabrication, and application of a thin porous multimodal pressure and temperature sensitive e-skin device by fully integrating it into the surface the Baxter Robot end effector utilizing an *in situ* fabrication method. The resulting device was capable of showing versatile functionality as a pressure sensor, temperature sensor, and heater. A multimodal measurement of temperature and pressure simultaneously with sensitivities of –800 ppm K^{-1} and 0.63% kPa^{-1} was achieved by the present device. The robust, flexible, and stretchable CNT and PAN materials were able to withstand over 1000 cycles with nearly no effects on the output signal. The fabrication strategy demonstrated in this work enables the development of multimodal sens-

ing capabilities in e-skins for soft robotics, intelligent artificial and human–machine interfaces.

7. Experimental Section/Methods

Sensor Fabrication and Material Process: The synthesis of PAN was performed using an electrospinning process with an application of 8 kV input voltage and a collecting speed of 500 rpm using the collector. The PAN (powder copolymer 99.5 %AN/0.5 %MA, Sigma Aldrich) was dissolved in dimethylformamide (N,N-dimethylformamide HCON(CH3)2, 99.0%, Sigma Aldrich) with a concentration of 10% (polymer/solvent). Highly oriented Multi-Wall CNT (MW-CNT) films were fabricated by pulling CNT fibres from a wafer of as-grown CNT forest. MW-CNTs with diameter of approx. 4–10 nm, length of 500 μm and high purity of carbon (>99.9%) were synthetized by the chemical vapor deposition technique [35].

Cycle Testing: The sensor device was reassembled to the Baxter robot's parallel gripper and cyclic testing was performed using a specialized program in the ROS environment. The parallel grippers were controlled to repetitively grip and release using the maximum gripping parameters available (100% grip acceleration, moving force, holding force, etc.) in 5 s intervals. Measurements were performed using an LCR Meter (U1733C) and recorded automatically using the Keysight GUI Data Logger Software.

Thermal Cycle Testing: To further analyse and characterize the potential for temperature sensing and the effects of temperature on pressure sensing, a temperature-controlled environment with precise control of the temperature of a gripped object was implemented. Dual Peltier modules (Adaptive Thermoelectric Generator Module GM250-127-14-16) attached to a solid aluminium block, with three embedded thermistors (STMicroelectronics LM335), was used as the gripped object. Multiple tests were performed to verify the effects of temperature and pressure on simultaneous resistance and capacitance measurements. A schematic diagram

of the experimental setup can be seen in Figure S6. The same method for gripping was used as in cyclic testing.

Declaration of Competing Interest

The authors declare that they have no known competing financial interests or personal relationships that could have appeared to influence the work reported in this paper.

Acknowledgements

Data availability statement

The raw/processed data required to reproduce these findings cannot be shared at this time as the data also forms part of an ongoing study.

Appendix A. Supplementary material

Supplementary calibration, alternate mode, and setup figures are available in compliment to the main text data.

Supplementary data to this article can be found online at https://doi.org/10.1016/j.matdes.2021.109886.

References

[1] M. Jindai, T. Watanabe, S. Shibata, T. Yamamoto, Development of a handshake robot system for embodied interaction with humans, in: ROMAN 2006-The 15th IEEE International Symposium on Robot and Human Interactive Communication, IEEE, 2006, pp. 710–715.

[2] G. Wang, Y. Yu, Q. Feng, Design of end-effector for tomato robotic harvesting, IFAC-PapersOnLine 49 (16) (2016) 190–193.

[3] V. Cortés et al., Integration of simultaneous tactile sensing and visible and near-infrared reflectance spectroscopy in a robot gripper for mango quality assessment, Biosyst. Eng. 162 (2017) 112–123.

[4] L. Scimeca, P. Maiolino, D. Cardin-Catalan, A. P. del Pobil, A. Morales, F. Iida, Non-Destructive Robotic Assessment of Mango Ripeness via Multi-Point Soft Haptics, in: 2019 International Conference on Robotics and Automation (ICRA), IEEE, 2019, pp. 1821–1826.

[5] J. Iqbal, Z.H. Khan, A. Khalid, Prospects of robotics in food industry, Food Sci. Technol. 37 (2) (2017) 159–165.

[6] J. Tegin, J. Wikander, Tactile sensing in intelligent robotic manipulation–a review, Ind. Robot: Int. J., 2005.

[7] M. Zhu, T. He, C. Lee, Technologies toward next generation human machine interfaces: From machine learning enhanced tactile sensing to neuromorphic sensory systems, Appl. Phys. Rev. 7 (3) (2020) 031305.

[8] T. Someya, M. Amagai, Toward a new generation of smart skins, Nat. Biotechnol. 37 (4) (2019) 382–388.

[9] B. Dong et al., Technology evolution from self-powered sensors to AIoT enabled smart homes, Nano Energy 79 (2020) 105414.

[10] Y. Guo, S. Gao, W. Yue, C. Zhang, Y. Li, Anodized Aluminum Oxide-Assisted Low-Cost Flexible Capacitive Pressure Sensors Based on Double-Sided Nanopillars by a Facile Fabrication Method, ACS Appl. Mater. Interfaces 11 (51) (2019) 48594–48603.

[11] W. Asghar et al., Piezocapacitive Flexible E-Skin Pressure Sensors Having Magnetically Grown Microstructures, Adv. Mater. Technol. 5 (2) (2020) 1900934.

[12] Y. Gao, C. Lu, Y. Guohui, J. Sha, J. Tan, F. Xuan, Laser micro-structured pressure sensor with modulated sensitivity for electronic skins, Nanotechnology 30 (32) (2019) 325502.

[13] S. Wang, K.-H. Huang, Y.-J. Yang, A Highly Sensitive Capacitive Pressure Sensor with Microdome Structure for Robot Tactile Detection, in: 2019 20th International Conference on Solid-State Sensors, Actuators and Microsystems & Eurosensors XXXIII (TRANSDUCERS & EUROSENSORS XXXIII), IEEE, 2019, pp. 458–461.

[14] J.C. Yang et al., Microstructured porous pyramid-based ultrahigh sensitive pressure sensor insensitive to strain and temperature, ACS Appl. Mater. Interfaces 11 (21) (2019) 19472–19480.

[15] D. Kwon et al., Highly sensitive, flexible, and wearable pressure sensor based on a giant piezocapacitive effect of three-dimensional microporous elastomeric dielectric layer, ACS Appl. Mater. Interfaces 8 (26) (2016) 16922–16931.

[16] J. Jia, G. Huang, J. Deng, K. Pan, Skin-inspired flexible and high-sensitivity pressure sensors based on rGO films with continuous-gradient wrinkles, Nanoscale 11 (10) (2019) 4258–4266.

[17] S. Chun, J. Kim, C. Pang, A transparent, glue-free, skin-attachable graphene pressure sensor with micropillars for skin-elasticity measurement, Nanotechnology 30 (33) (2019) 335501.

[18] T. Yamaguchi, T. Arie, S. Akita, K. Takei, Electronic Skin-Integrated Soft Robotic Hand, in: 2019 20th International Conference on Solid-State Sensors, Actuators and Microsystems & Eurosensors XXXIII (TRANSDUCERS & EUROSENSORS XXXIII), IEEE, 2019, pp. 543–546.

[19] T. Yamaguchi, T. Kashiwagi, T. Arie, S. Akita, K. Takei, Human-Like Electronic Skin-Integrated Soft Robotic Hand, Adv. Intell. Syst. 1 (2) (2019) 1900018.

[20] G. Franchi, A. ten Pas, R. Platt, S. Panzieri, The Baxter Easyhand: A robot hand that costs $150 US in parts, in: 2015 IEEE/RSJ International Conference on Intelligent Robots and Systems (IROS), IEEE, 2015, pp. 2917–2922.

[21] R. Hayakawa, T. Nishi, K. Arisawa, Y. Wada, "Dielectric relaxation in the paracrystalline phase in polyacrylonitrile," Journal of Polymer Science Part A-2: Polymer, Physics 5 (1) (1967) 165–177.

[22] C. Parker, J.-P. Maria, A. Kingon, Temperature and thickness dependent permittivity of (Ba, Sr) TiO 3 thin films, Appl. Phys. Lett. 81 (2) (2002) 340–342.

[23] J. Fastier-Wooller, T. Dinh, D.V. Dao, Soft ionic liquid multi-point touch sensor, RSC Adv. 9 (19) (2019) 10733–10738.

[24] A.W. Friend, Charts of Dielectric Constant or Refractive Index of the Troposphere, Bull. Am. Meteorol. Soc. 29 (10) (1948) 500–509.

[25] A. Gupta, R. Singhal, V. Agarwal, Effect of heat treatment on dielectric relaxation of polyacrylonitrile: Reversible thermally induced structural change, J. Appl. Polym. Sci. 26 (11) (1981) 3599–3608.

[26] T. Dinh et al., Environment-friendly carbon nanotube based flexible electronics for noninvasive and wearable healthcare, J. Mater. Chem. C 4 (42) (2016) 10061–10068.

[27] T. Dinh et al., Polyacrylonitrile-carbon Nanotube-polyacrylonitrile: A Versatile Robust Platform for Flexible Multifunctional Electronic Devices in Medical Applications, Macromol. Mater. Eng. 304 (6) (2019) 1900014.

[28] X. Zhang, W. Lu, G. Zhou, Q. Li, Understanding the mechanical and conductive properties of carbon nanotube fibers for smart electronics, Adv. Mater. 32 (5) (2020) 1902028.

[29] V. Dau, C.-D. Tran, T.T. Bui, V. Nguyen, T. Dinh, Piezo-resistive and thermo-resistance effects of highly-aligned CNT based macrostructures, RSC Adv. 6 (108) (2016) 106090–106095.

[30] S. Senthilkumar, S. Rajesh, A. Jayalakshmi, D. Mohan, Biocompatibility studies of polyacrylonitrile membranes modified with carboxylated polyetherimide, Mater. Sci. Eng., C 33 (7) (2013) 3615–3626.

[31] C.-D. Tran, K. Le-Cao, T.T. Bui, Dielectrophoresis can control the density of CNT membranes as confirmed by experiment and dissipative particle simulation, Carbon 155 (2019) 279–286.

[32] C.-D. Tran, W. Humphries, S.M. Smith, C. Huynh, S. Lucas, Improving the tensile strength of carbon nanotube spun yarns using a modified spinning process, Carbon 47 (11) (2009) 2662–2670.

[33] Y. Taminami, S. Yokota, A. Matsumoto, D. Chugo, H. Hashimoto, Effects of the Heartbeat Expression to Remote Presence by Shaking Hands With a Remote-Controlled Robot Hand and Review of its Parameters, in: 2020 IEEE/SICE International Symposium on System Integration (SII), IEEE, 2020, pp. 444–448.

[34] E. Park, J. Lee, I am a warm robot: the effects of temperature in physical human–robot interaction, Robotica 32 (1) (2014) 133–142.

[35] C.P. Huynh, S.C. Hawkins, Understanding the synthesis of directly spinnable carbon nanotube forests, Carbon 48 (4) (2010) 1105–1115.